JOURNAL OF GEOPHYSICAL RESEARCH, VOL. 101, NO. A12, PAGES 26,783-26,793, DECEMBER 1, 1996

Coordinated measurements of *F* region dynamics related to the thermospheric midnight temperature maximum

M. Colerico,[1,2] M. Mendillo,[1,2] D. Nottingham,[1] J. Baumgardner,[1] J. Meriwether,[3] J.Mirick,[3] B. W. Reinisch,[4] J. L. Scali,[4] C. G. Fesen,[5] and M. A. Biondi[6]

Abstract. As part of the NSF/CEDAR program (Coupling Energetics, and Dynamics of Atmospheric Regions) in Multi-Instrumented Studies of Equatorial Thermospheric Aeronomy (MISETA), an all-sky CCD airglow imaging system has been in operation in Arequipa, Peru, since October 1993. Here we report on the first such use of a wide-field imager to document the optical signature and variability of a brightness feature associated with the so-called midnight temperature maximum (MTM). While the observational driver of this study is a "brightness wave" (BW) seen in 6300 Å and 5577 Å airglow images, detailed case studies are conducted during two campaign periods when Fabry-Perot interferometer (FPI) and digital ionosonde data were also available. During the passage of a BW, the FPI observed enhancements in thermospheric temperatures, reversals (from equatorward to poleward) of the meridional neutral winds, and local minima in the zonal neutral winds. The ionosonde recorded decreases in the height of the F- layer during BW events. This lends support to the concept that the poleward winds generated by the MTM pressure bulge cause the lowering of the F- layer to regions of enhanced loss (h < 300 km) and corresponding airglow production. The two-dimensional field -of -view of the imager allows identification of the geographical orientation of the BW pattern. We use the orientation angle of the BW as an indicator of the geographical orientation of the MTM. Significant day-to-day variability in these patterns suggest a complex mix of tidal mode interactions that lead to the overall MTM phenomena.

Introduction

The midnight temperature maximum (MTM) is an enhancement in the thermal structure of the upper atmosphere that occurs during nighttime hours at low latitudes. *Spencer et al.* [1979] reported the first in- situ measurements of the MTM using the Neutral Atmospheric Temperature Experiment (NATE) instrument aboard the Atmosphere Explorer- E (AE-E) satellite. Simultaneous thermospheric wind measurements from the AE-E satellite revealed a correlation between the MTM and a reversal or abatement in the meridional neutral winds from equatorward to poleward. This reversal/abatement in the meridional winds has been attributed to a pressure bulge which accompanies the MTM and serves as a mechanism for lowering the F- region to produce an enhancement in the oxygen 6300Å emission [*Herrero and Meriwether*, 1980]. Dynamics Explorer Satellite data [*Wharton et al.*, 1984] also revealed an abatement in the zonal neutral winds at low latitudes near local midnight. *Herrero et al.* [1985] interpreted this as evidence of the passage of the MTM.

Herrero and Spencer [1982] generated temperature maps for each season using the AE-E thermospheric temperature data in order to determine the seasonal variation of the MTM. As seen in Figure 1, the general pattern is an MTM centered on the geographic equator with two additional MTM features between 10° and 20° latitude in each hemisphere. The MTM occurs earlier and is more pronounced in the summer hemisphere than in the winter hemisphere, whereas during equinox months the MTM is generally symmetric about the geographic equator at approximately local midnight. One exception which is shown in the December solstice average temperature map is that in the southern hemisphere there are two regions of increased temperature, centered at approximately 2100 LT and 2400 LT, as opposed to the one region seen in the other maps.

The first Earth-based observations of an optical manifestation of the MTM were made by *Greenspan* [1966]. While measuring 6300Å zenith brightness using a photometer installed on the U.S. Naval Ship Croatan traveling from North to South America, Greenspan observed regular occurrences of an enhancement in the red line intensity near local midnight at equatorial latitudes. These enhancements were most pronounced in the latitude range from 0° to 15° S.

Nelson and Cogger [1971] identified the appearance of a 6300 Å postmidnight enhancement at Arecibo (18°N) with a downward descent of the ionosphere by 50 to 100 km which was called the midnight collapse. By studying the ionograms from a latitudinal chain of stations, they also showed that the

[1]Center for Space Physics, Boston University, Boston, Massachusetts.
[2]Also at Department of Electrical, Computer, and Systems Engineering, Boston University, Boston Massachusetts.
[3]Department of Physics and Astronomy, Clemson University, Clemson, South Carolina.
[4]Center for Atmospheric Research, University of Massachusetts, Lowell.
[5]Department of Physics and Astronomy, Dartmouth College, Hanover, New Hampshire.
[6]Department of Physics and Astronomy, University of Pittsburgh, Pittsburgh, Pennsylvania.

Paper number 96JA02337.
0148-0227/96/96JA-02337$09.00

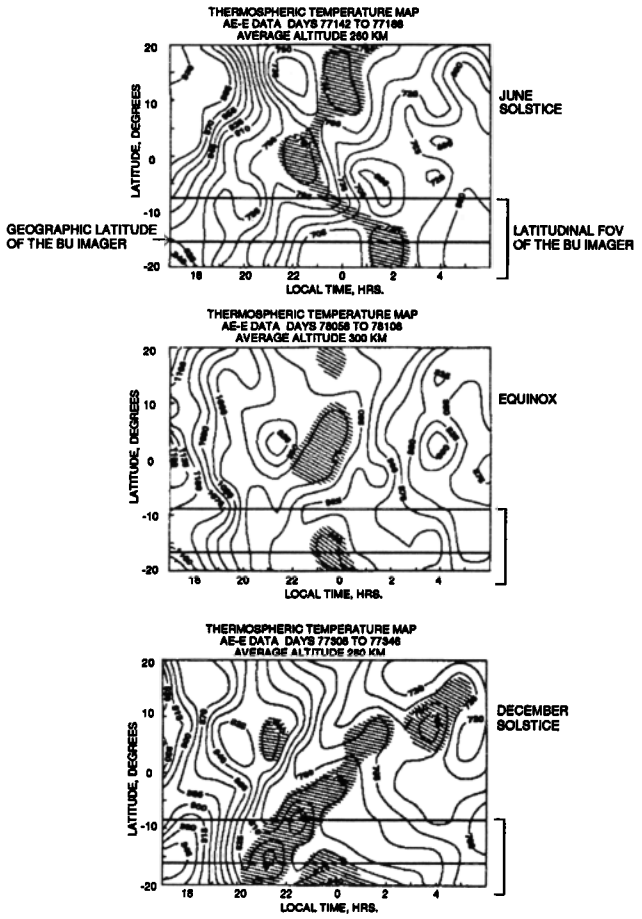

Figure 1. Thermospheric temperature maps showing midnight temperature maximum (MTM) patterns obtained from the Neutral Atmosphere Temperature Experiment (NATE) instrument onboard the Atmospheric Explorer (AE-E) satellite in 1977 [after *Herrero and Spencer*, 1982]. The field of view (FOV), in latitude, of 6300 Å airglow imaging observations made from Arequipa, Peru, is indicated to show how MTM patterns would enter the imager's FOV as Arequipa would rotate under such phenomena fixed in local time. Note that the AE-E data pertain to 1977 and mean monthly sunspot number (MMSN) of 28. The Arequipa imaging data come from 1993 and 1994, with MMSN = 55 and 30, respectively. For June Solstice, the MTM temperature contours (shaded regions) range from 720 °K to 780°K with the background temperature contours ranging from 690 °K to 750 °K. For equinox, the MTM temperature contours range from 950 °K to 975 °K with the background temperature contours ranging from 900 °K to 925 °K. For December solstice, the MTM temperature contours range from 750 °K to 840 °K with the background temperatures ranging from 720 °K to 825 °K.

local time of this vertical shift of the F- layer progressed systematically to later local times with larger latitudinal displacement from the equator. Radar studies of nighttime plasma dynamics by *Behnke and Harper* [1973] and *Harper* [1973] were successful in demonstrating that the cause of the downward motion of the F- layer was the progression of a pressure bulge that produced a reversal of the meridional component of the thermospheric winds. Such a change from the normally equatorwards flow to poleward flow lowers the F- layer peak due to the component of the meridional wind along the field line [*Friedman and Herrero*, 1981].

Mayr et al. [1979] showed theoretically that the formation of the midnight pressure bulge was likely to be a nonlinear interaction between the higher tidal modes of the thermospheric winds driven by solar in- situ forcing and the modulation of the electron density by the diurnal cycle of F-region ionization production. *Bamgboye and McClure* [1982] followed up the satellite observations of the midnight temperature anomaly with a study that used nighttime electron temperature measurements from the Jicamarca Radar Observatory to determine the climatology of the local time dependence of the observed maximum temperature perturbation. This work found a systematic seasonal variation of the MTM in which the MTM appeared during local winter at times after midnight, for equinox conditions at times near local midnight and for local summer conditions at times near 2100-2200 LT. The history of this work has been reviewed by *Herrero et al.* [1993] providing extensive details of the physics of this interesting feature of the low-latitude thermosphere.

In this paper, we explore several aspects of transient airglow features to determine if they are the first two-dimensional detection of the F- region's optical signature of the MTM. Central to this effort is the use of coordinated Fabry-Perot interferometer (FPI) and ionosonde observations to provide the dynamical parameters needed to link the airglow patterns to an MTM origin.

Observations

Imager Observations

As part of the NSF/MISETA Program (Multi-Instrumented Studies of Equatorial Thermospheric Aeronomy), an all-sky, image-intensified CCD camera system [*Baumgardner et al.*, 1993] has operated in Arequipa, Peru (16.2°S, 71.35°W) since October 1993. Figure 2 illustrates the field of view (FOV) for this system when observing oxygen 6300 Å airglow patterns at approximately 300 km. The MISETA imaging system is equipped with three oxygen line filters: 5577 Å, 6300 Å, and 7774 Å. An example of a transient 6300Å airglow feature (called a brightness wave (BW) by *Mendillo et al.*, [1996]) moving through the field of view is shown in Figure 3. Observations show that the BW is present in both the 5577Å and 6300Å wavelengths, but not in 7774Å, implying that the phenomenon originates at altitudes below the height of peak F- region electron density (h_{max}). The stationary bright region on the northwest edge of the images in Figure 3 is due to the city lights of Arequipa and has no relationship to the passage of the BW. Note that the onset of the effect in the northeast is somewhat poorly defined in comparison to its appearance at zenith and subsequent exit to the southwest. The most common observance time for this phenomena is centered on local midnight (0500 UT) for enhancements moving in the poleward direction; at times it is preceded by an additional event moving equatorward at approximately 2100 LT. These events generally occur over a time period of 1 - 2 hours.

The seasonal dependence of the BW has been determined from analysis of a sizable database of images (October 1993 to March 1995). As shown in Figure 4, the BW seems to occur most frequently during the equinox periods with the September - October equinox having the higher occurrence rate. For this reason, we will use the two equinox periods (MISETA- pilot campaign of October 8-22, 1993 , and the

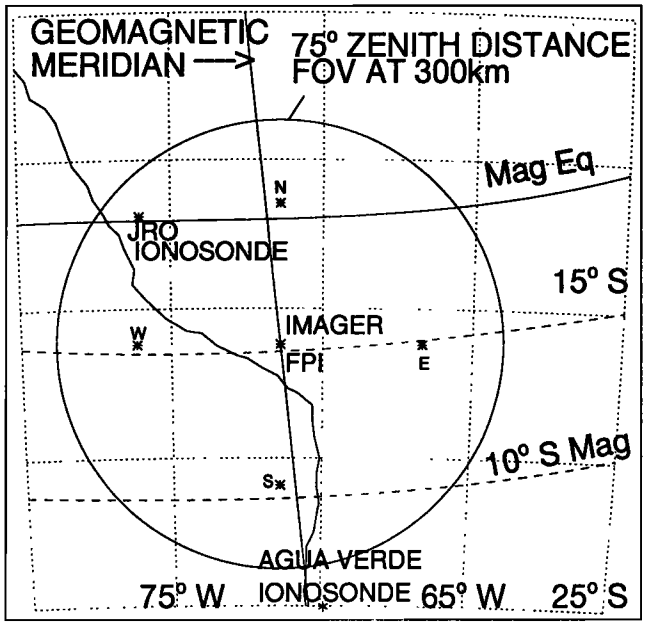

Figure 2. The field of view (FOV) sampled by the MISETA all-sky imager in Arequipa, Peru, for 6300 Å oxygen airglow using an average emission height of 300 km. The locations of a Fabry-Perot interferometer (FPI) and ionosondes at the Jicamarca Radio Observatory (JRO) and at Agua Verde (Chile) are shown. The measurement points, north (N), south (S), east (E), west(W) with a zenith angle of 60° and zenith, for the FPI are shown within the FOV of the imager by asterisks.

MISETA-I campaign of September 23 to October 9, 1994) as our case study periods in this paper.

During the MISETA- pilot campaign, eight out of nine clear evenings had occurrences of the BW. Typically, events centered on local midnight were found during this period, an example of which was shown in Figure 3. The AE-E equinox temperature map in Figure 1b shows a single MTM centered at 16° S, spanning 1-2 hours at local midnight, consistent with the BW feature captured in the Arequipa images during the October 1993 period.

The MISETA-I campaign also showed a high occurrence rate of BW events at local midnight and, in most cases, by the additional occurrence of a BW earlier in the evening. The pre-midnight events are generally weaker in brightness than the local midnight events (e.g., ~150 Rayleighs (R) above background versus 250 R). An example of the premidnight pattern is shown in Figure 5. In contrast to the October 1993 results, there is not an agreement between the AE-E temperature maps for equinox and the twin occurrence times and durations of the airglow BW events for the October 1994 period. Specifically, the equinox temperature map (Figure 1b) does not contain an earlier MTM to correlate with the earlier BW. From an aeronomic perspective, the transition between seasons can vary from year to year [*Carlson and Crowley* 1989]. Thus a comparison was made between the following season (December solstice) temperature map (Figure 1c) and the October 1994 BW data set. The December solstice temperature map shows two MTMs that occur between 2000LT - 2200LT and 2300LT - 0100LT, both having a time duration of 1-2 hours. These are consistent with the times of

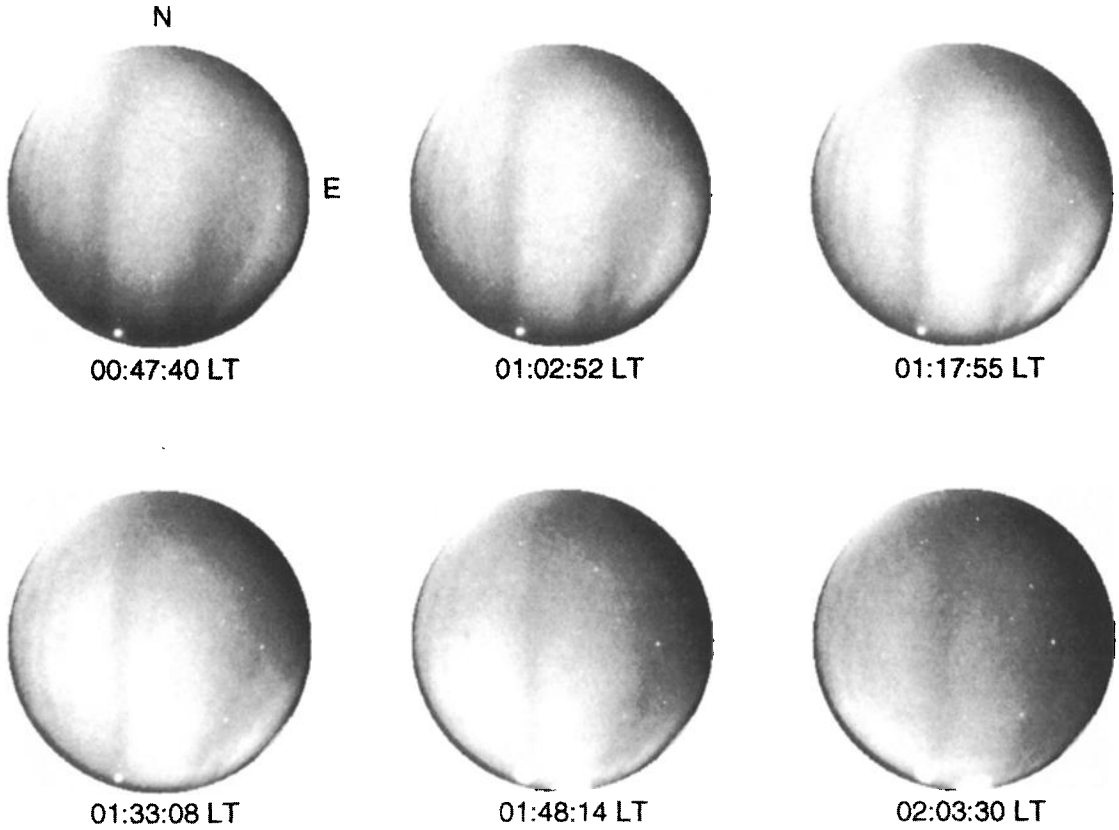

Figure 3. A sequence of six images taken with the MISETA all-sky imager at Arequipa, Peru, on the evening of October 14, 1993, which illustrates the midnight occurrence of a brightness wave (BW) event in the 6300 Å wavelength. Note that the stationary bright region at the northwest edge of the images is due to the city lights of Arequipa and is not related to BW events.

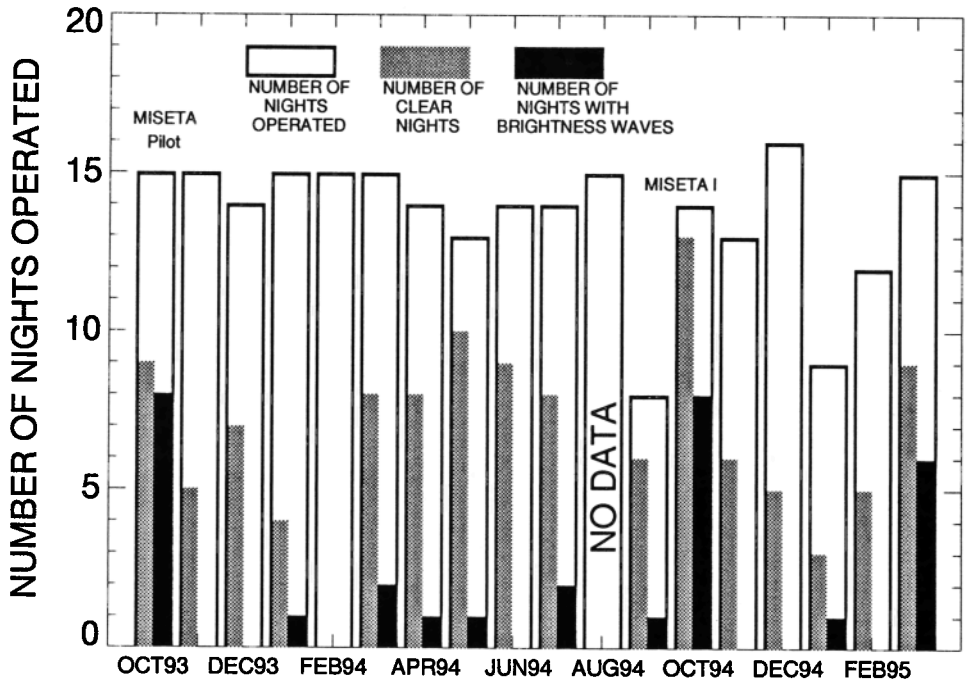

Figure 4. Sky conditions and BW activity summary for MISETA all-sky imager data taken from October 1993 to March 1995. The occurrence rate of BW events is highest during equinox periods (September-October, March-April) with the September-October equinox having a consistently higher occurrence rate. There is a noticeable lack of brightness wave events during December solstice periods, in contrast to the AE-E patterns for MTM occurrence shown in Figure 1c. Sky conditions limit the number of observations during November, December, and January.

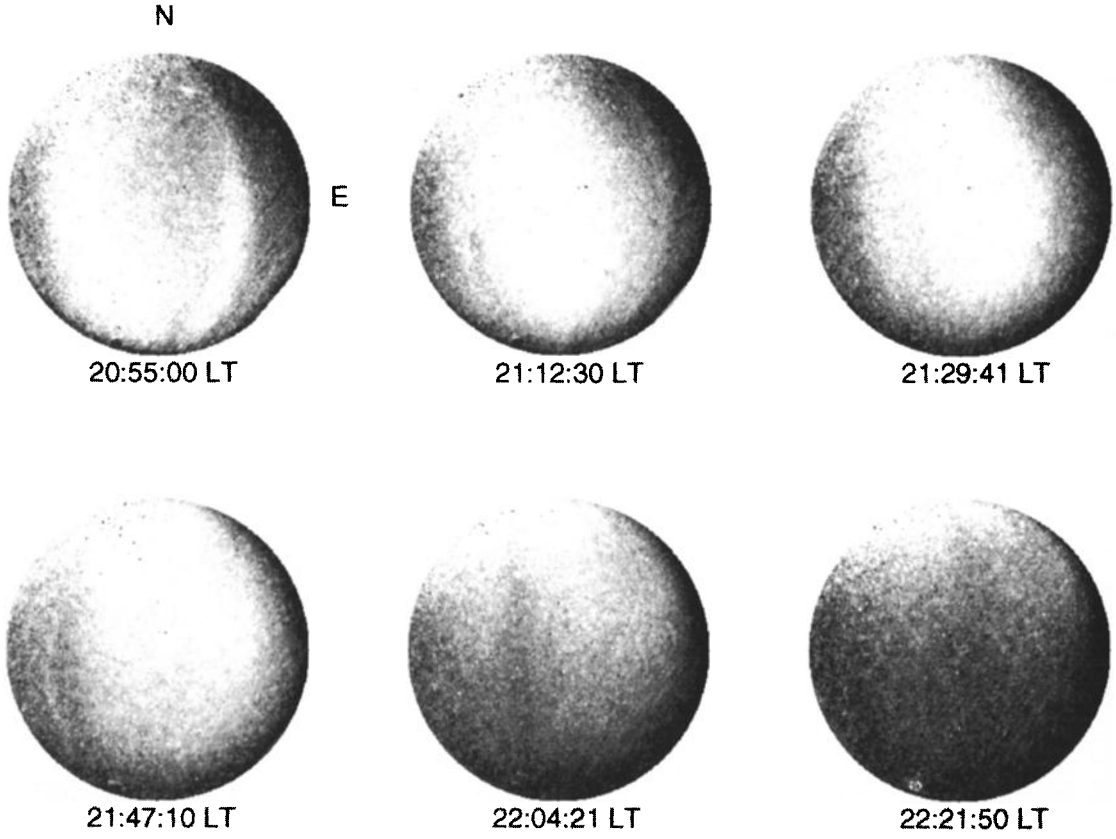

Figure 5. A sequence of six images taken with the MISETA imager on the evening of October 1, 1994, which illustrates the premidnight occurrence of a BW event.

occurrence and duration of the two airglow BW features found in the Arequipa October 1994 data set.

Meridional scans of the 6300 Å airglow images offer a concise way to show the BWs over the course of an evening and to aid in the calculation of their apparent velocities. Meridional brightness scans are constructed by taking a north - south (latitudinal) slice out of the center of each image obtained in the course of an evening. These latitudinal slices are stacked in chronological order resulting in a latitude versus time plot that reveals the BW in a format identical to that used for the AE-E thermospheric temperature maps. The latitudinal range covered by the imager is 8° to 23° S, and useful images can be obtained each night from 1930 - 0330 LT. Results for the night of October 13-14, 1993, are shown in Figure 6a and for October 1-2, 1994, in Figure 6b. Comparison of the meridional brightness scans in Figures 6a and 6b with the temperature maps in Figures 1b and 1c, respectively, show good agreement in terms of time of occurrence, duration of the event, geographic location and the orientation of the features. This supports the concept that the 6300 Å BW in the Arequipa MISETA image is an optical signature of the MTM phenomena.

Finally, the apparent meridional velocity at which the BW feature moves through the field of view can be easily determined using the meridional intensity scans by calculating the slope of the latitude of peak brightness versus time. As described by *Mendillo et al.* [1996], this is done by applying curve-fitting techniques to the times of peak brightness at 1° intervals over the range 12° - 20° S latitude (corresponding to zenith angles of 60°, i.e., to the central two- thirds of the all-sky FOV). The resultant slopes and derived speeds are summarized in Figure 7. The average poleward speed for October 1993 midnight BW (MBW) events was 248 m/s, whereas the average speed for October 1994 events was 356 m/s. The average equatorward speed for premidnight BW (PMBW) events, seen only in the October 1994 data set, was 368 m/s. In a later section, we combine this apparent meridional speed and the Earth's corotation speed to obtain geographic orientations of the MTM effect, as shown in the Figure 1 temperature results.

FPI Observations

A Fabry-Perot interferometer (FPI) has operated in Arequipa since 1983 [*Meriwether et al.*, 1986]. There has been a rich yield of scientific results from this instrument [e.g., *Biondi et al.*, 1991, 1995]. This FPI, upgraded for MISETA studies, was in operation during both the MISETA-pilot and MISETA-I campaigns and made coincident measurements with the imaging system on several nights. The

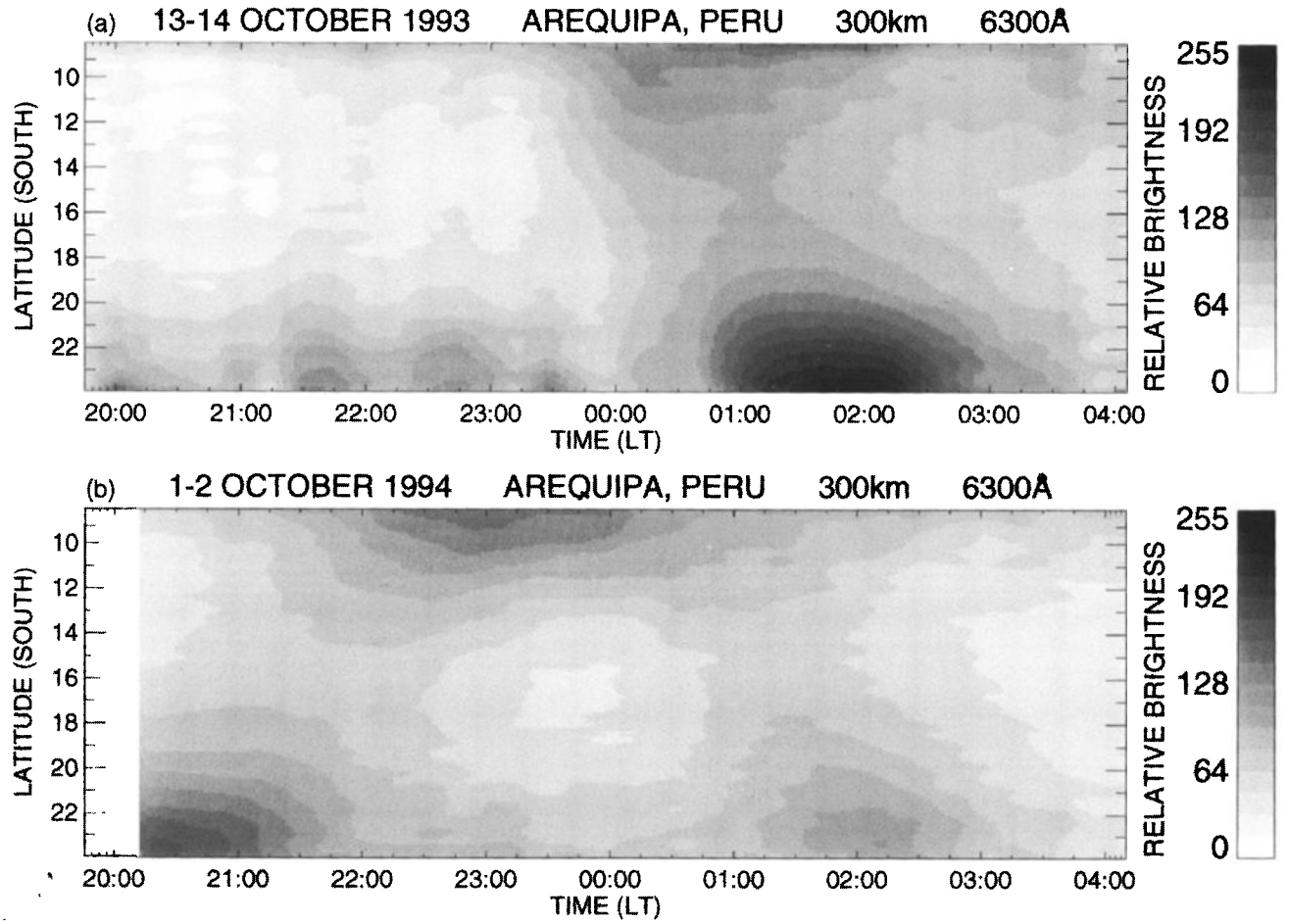

Figure 6. Meridional intensity scans for (a) October 13-14, 1993, and (b) October 1-2, 1994, illustrate the equatorward and poleward movement of the premidnight and midnight BW events, respectively. These meridional intensity scans compare favorably with the equinox and December solstice AE-E thermospheric temperature maps given in Figures 1b and 1c, respectively.

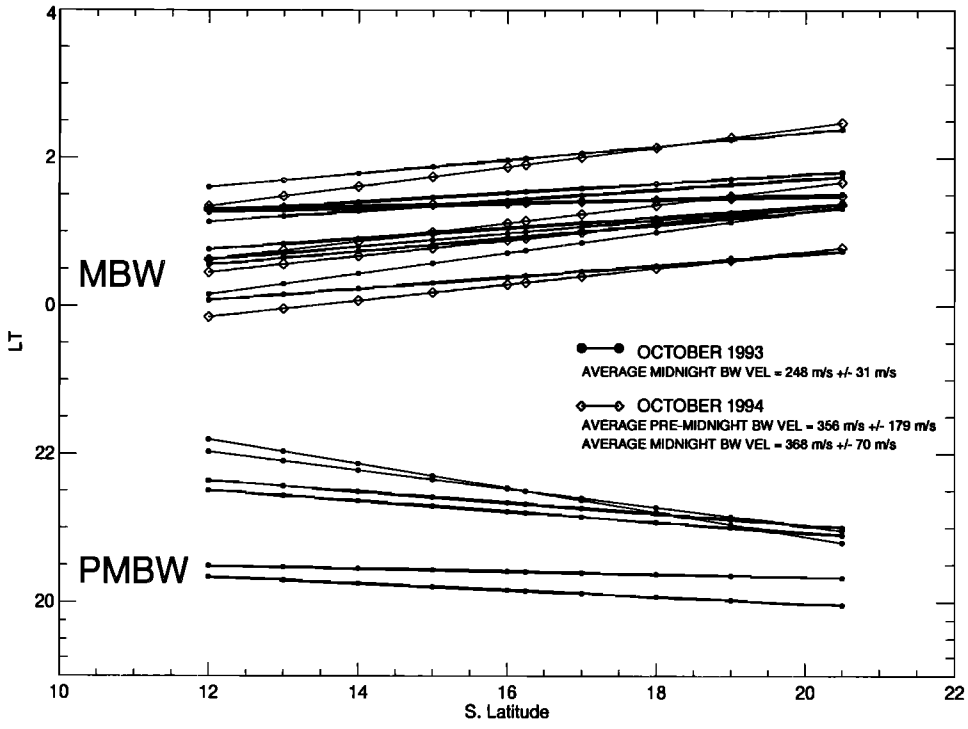

Figure 7. Summary of BW apparent motion for both the October 1993 and October 1994 equinox periods showing the variability in the velocity, time of occurrence, and duration of BW events. The pre-midnight brightness wave (PMBW) moves equatorward, while the midnight brightness wave (MBW) moves poleward.

FPI makes measurements in the North, South, East, and West directions at a zenith angle of 60°, as well as measurements at zenith. To illustrate BW signatures in the FPI observations, Figure 8 shows meridional wind measurements made on October 1-2, 1994, from the north and south directions. These show the temporal progression of two reversals in the meridional winds. For the first case, a reversal is seen in the southern measurements (lower panel) at 1906 LT, followed by its appearance in the northern measurements at 2012 LT. This is consistent with the passage of a PMBW which enters in southwest and exits to the northeast (as shown in Figure 5 and Figure 6b). The opposite is true for the second observed reversal. The reversal is first seen in the northern measurement at approximately 2350 LT, followed by its detection at 0155 LT in the south. This is consistent with the passage of a MBW which appears first in the northeast and exits to the southwest (as shown in the October 2, 1994, data in Figure 6b).

Additional comparisons were made between the FPI and imager data sets, on a night-by-night basis, for both campaigns. During the MISETA- pilot campaign, coincident measurements were conducted on three evenings, October 14, 15, and16, 1993. As shown in Figure 9, FPI events consisting of a minimum in the zonal winds, reversal/abatement in the meridional winds, and a local maximum in the neutral temperature occurred once over the course of each evening, and these correlated with the passage of a BW. During the MISETA-I campaign, coincident measurements were made from September 30 to October 6, 1994, and on October 9, 1994, as shown in Figure 10. This is a far more complete data set to support night-to-night comparisons between the FPI and imager patterns. On most evenings, the FPI meridional wind reversals (or hints thereof) were seen twice : between 2000-

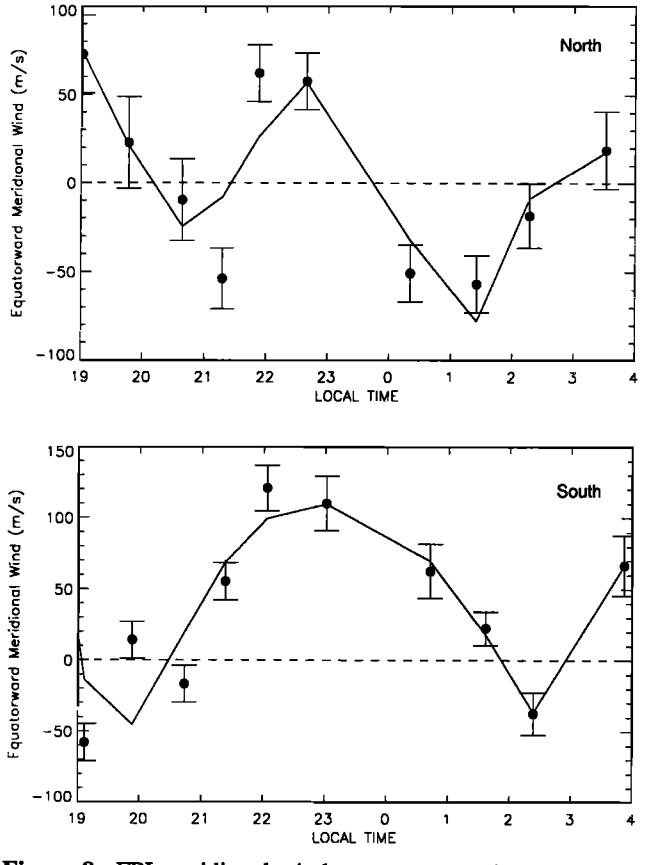

Figure 8. FPI meridional wind measurements for October 1-2, 1994, demonstrating a temporal progression in the observation of two reversals of the meridional winds.

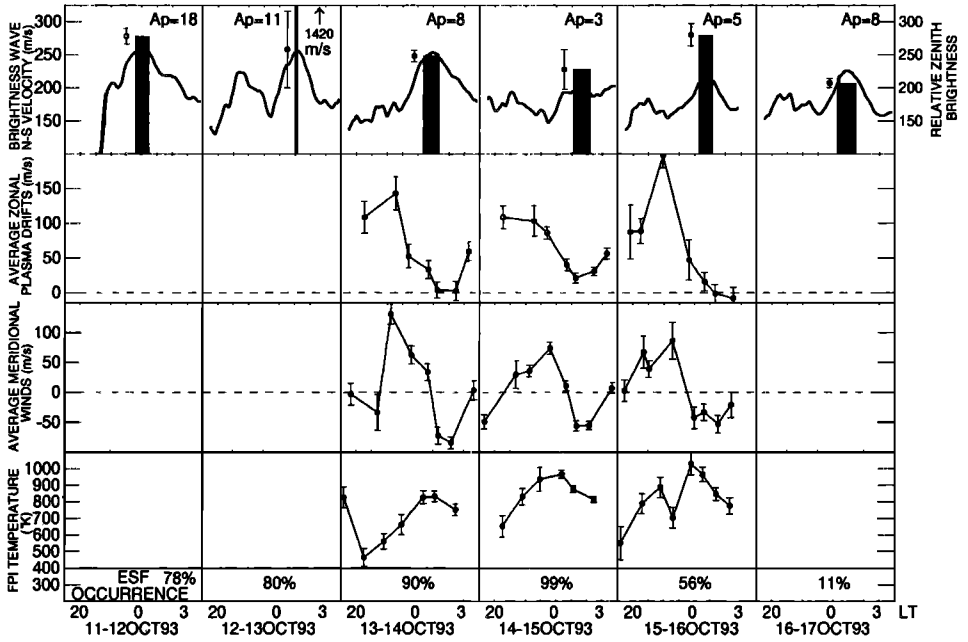

Figure 9. Summary of imager and Fabry-Perot (FPI) data for October 12-17, 1993. The top panel gives the relative zenith brightness in 6300 Å (solid line) and the magnitude of the BW apparent meridional velocity (with error bars) from the imager, as well as values of the daily geomagnetic index Ap. FPI observations of zonal and meridional neutral wind speeds (positive equatorward and eastward) appear in the next two panels, with FPI neutral temperatures in the fourth panel. The occurrence of equatorial spread- F (ESF) associated airglow depletions seen in the imager are also shown for geophysical context. Note the correlation of midnight BW events with dips in the zonal winds, reversals/abatements in the meridional winds, and a local maximum in neutral temperature, and that these are not related in any significant way to changes in Ap or ESF activity.

2200LT and 2300-0100LT, again coincident with the BW passage. As in Figure 9, and as will be discussed below, the temperature enhancements are particularly prominent in these data sets.

Ionosonde Measurements

A digital ionosonde [*Reinisch*, 1995] has been in operation near the geomagnetic equator at Jicamarca, Peru (12°S, 77°

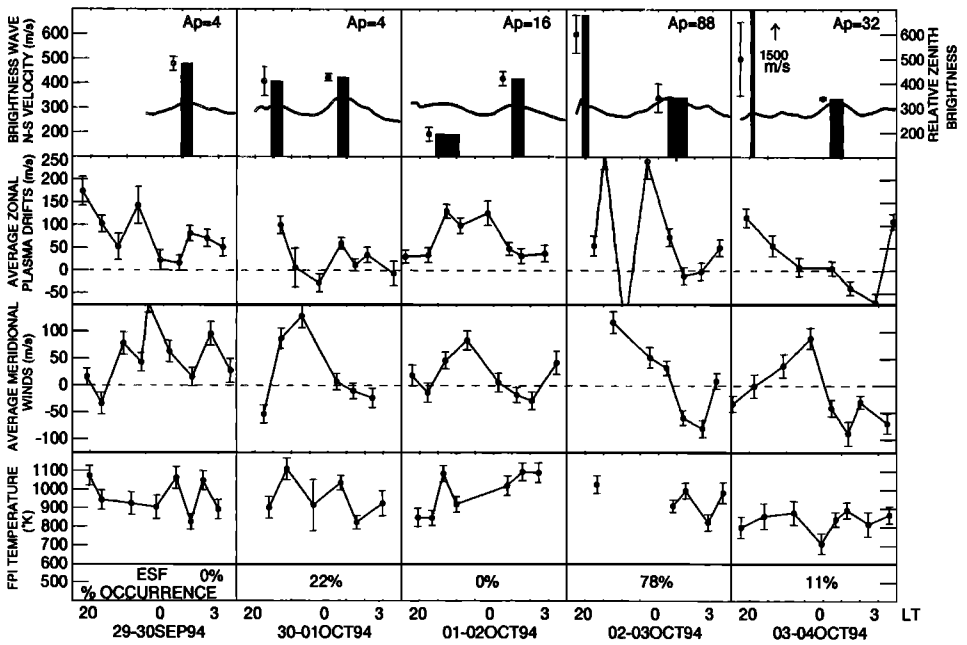

Figure 10. Summary of BW imager data and FPI data for September 30 to October 4, 1994, using the same format as Figure 9. Note the correlation of both premidnight and midnight BW events with local minima in the zonal winds, reversals/abatements in the meridional winds, and local maxima in the neutral temperatures.

W), since March 1992. Prior to the MISETA program, this instrument has been used in several studies of equatorial ionospheric behavior and is used in several MISETA papers in this special section. During the MISETA- pilot campaign period, the ionosonde data show a small drop in h_{max} to an altitude between 250 and 300 km at approximately local midnight with a duration from 1 to 2 hours (see Figure 11a). Given that Jicamarca is essentially at the dip equator, vertical motions driven by horizontal winds should be negligible. Vertical plasma drifts due to electric fields typically show average patterns of downward drift all night [*Fejer et al.*, 1991], with no particular prominence near midnight. Recalling that BW signatures are poorly defined at the geomagnetic equator, it is impossible to relate airglow production and plasma dynamics at that site without knowledge of electric field effects; unfortunately, no such observations were made by the Jicamarca ISR. Thus, we simply note that for the MISETA- pilot data, there was a decent of h_{max} to airglow producing altitudes at Jicamarca, prior to a BW moving poleward through zenith at Arequipa. Clearly, an ionosonde at a more southerly site was needed.

During the MISETA-I campaign, the University of Massachusetts at Lowell operated an additional ionosonde at Agua Verde (25.4° S, 70° W) from September 30 to October 4, 1994. As shown in Figure 2, Agua Verde is at the southern edge of the imager's field of view. The October 1994 data set exhibited both pre-midnight and midnight brightness waves. In Figure 11b, two-site ionosonde data are given for a premidnight example of the brightness wave. It is difficult to identify any consistent patterns in h_{max} at Jicamarca on these nights. The Agua Verde data, however, show decreases in h_{max} between 2000-2200 LT consistent with an equatorward propagation of the BW. In Figure 11c, both premidnight and midnight drops in h_{max} at Agua Verde occur on October 2 that correlate with the two brightness wave events seen that night. The h_{max} decrease at Agua Verde, with negligible effects at Jicamarca, lend support for a wind induced motion. This is due to field geometry since Agua Verde has a dip angle of -21.5° (IGRF 1990 at 300 km) allowing for greater vertical motion of the F- layer by meridional winds. From this use of the ionosonde data, we now have supporting evidence that the reversal of the meridional winds seen by the Arequipa FPI are indeed serving as a mechanism for lowering the F-layer to produce the BW in the region of the MTM. In future campaigns, we plan to request Jicamarca ISR observations of plasma drifts and temperatures to explore mechanisms in more comprehensive and quantitative ways than is possible with the 1993-1994 data set.

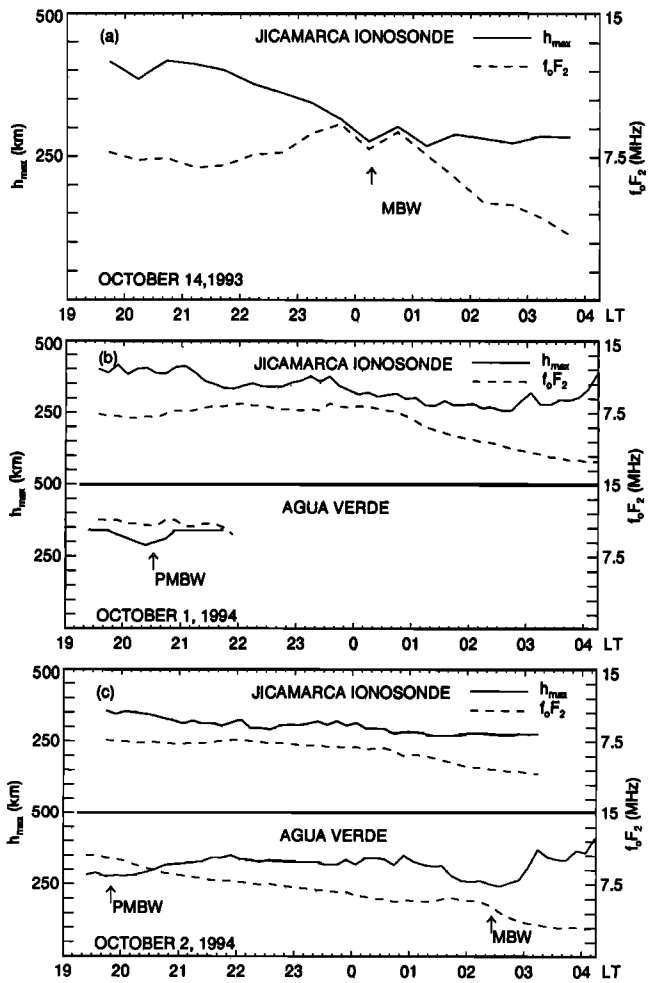

Figure 11. Ionosonde h_{max} and f_0F_2 measurements, taken at the Jicamarca Radio Observatory (JRO) for October 14, 1993, and at JRO and Agua Verde for October 1-2, 1994, showing dips in the F- layer height to 250-300 km during BW events.

Summary Of Observations

The MISETA imager sees a BW move through its field of view between 2000-2200 LT and 2300-0100 LT. For the earlier brightness wave, seen consistently in the MISETA-I data set, the direction of motion is south to north (equatorward). The later brightness wave event, seen in both campaigns, passes from north to south (poleward) through the field of view. In each instance, the FPI data suggest a local minimum in the zonal winds, a reversal in the meridional winds from equatorward to poleward, and a local maximum in the neutral temperature. Simultaneously, ionosonde data show a decrease in the height of the F- region. The times of occurrence for all BW events in the MISETA- pilot campaign are consistent with the AE-E data for the average location of the MTM in geographic latitude and local time under equinox conditions. The BW morphology from the MISETA-I campaign agrees with the AE-E data for December solstice conditions. A scenario that unifies these effects is one where the pressure bulge that accompanies an MTM event serves to reverse the normally equatorward meridional winds and lower the F- region. This lowering of the F- region produces an enhancement in the O I 6300 Å emission seen by the imager. While the appearance of the brightness wave shows an equatorward motion for the premidnight case and poleward motion for the midnight case, both are due to disturbance winds that are poleward (i.e., away from the pressure bulge). It is the geographic orientation angle of the MTM feature (θ, described below) that determines these differences in apparent meridional directions, not the winds themselves.

Discussion

We now address the apparent direction of motion of the BW. As shown in Figure 1, the MTM is stationary in local time and may be tilted either eastward or westward with respect to the north-south meridian. All of the instruments

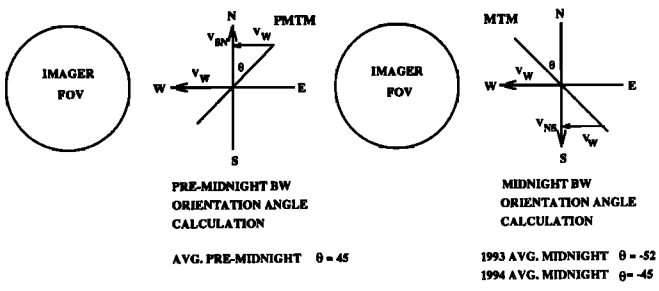

Figure 12. Definition of the angle of orientation, θ, with respect to the north-south meridian for both premidnight and midnight BW events. Average θ results for premidnight temperature maximum (PMTM) and midnight temperature maximum (MTM) patterns are indicated.

move through this MTM feature at the corotation speed of the Earth. Figure 12 offers an illustration of the relevant geometry. Depending on the angle of orientation (θ) of the MTM, more southerly or northerly instruments would see it first. Using the BW as a tracer for MTM driven events, we can calculate the MTM's angle of orientation (θ). For the case of the premidnight occurrence, the equatorward movement of the BW would indicate that the MTM event has an eastward tilt (i.e. a positive orientation angle, θ, with respect to the north-south meridian). For the case of a midnight occurrence, the poleward motion of the BW would indicate that the MTM is tilted westward. The orientation of the MTM pattern (assumed planar and of finite width, as suggested by Figure 1.) can be calculated from the velocity at which the BW moves through the field of view, via $\theta = \tan^{-1}(V_w/V_{ns})$, where V_w is equivalent to the Earth's corotation speed and V_{ns} is the apparent meridional velocity at which the BW moves through the field of view of the imager. V_{ns} is obtained each night from the slope of the latitude vs. time meridional brightness pattern, as shown in Figures 6 and 7. There is considerable variability in the derived angles, ranging from 12° to 67°. The average angle of orientation of the MTM for the MISETA-0pilot campaign was calculated to be 52° westward. For the MISETA-I campaign, the average angles of orientation for the pre-midnight and midnight occurrences were 45°eastward and 45° westward, respectively.

The extraction of the MTM orientation angle (θ) has its uncertainties, due mainly to the fact that the brightness wave is poorly defined near the geomagnetic equator where neutral winds cause negligible vertical plasma motion. Also, it remains to be seen how day-to-day values of θ can be used to understand the tidal mode sources and interactions that lead to the MTM. Yet, given that the main source of spatial information on MTM structure and dynamics has, until now, been from limited satellite data, the imaging science results reported on here offer avenues for additional research on these topics.

The types of MTM effects reported here have not yet been modeled fully. We assess the status of modeling in two ways: with an empirical neutral atmosphere model, MSIS-86 [*Hedin*, 1991], and by a first principles state-of-the-art numerical model, the National Center for Atmospheric Research thermosphere-ionosphere-electrodynamical general circulation model (TIEGCM) [*Richmond et al.*, 1992]. The models were run for the MISETA-I campaign for both magnetically quiet and mildly disturbed conditions (Ap = 3 and Ap = 22) with low solar flux (F10.7 = 82). Figure 13 shows the results from the model runs. Both models predict an MTM event at approximately local midnight but much smaller in magnitude (10 - 40 °K) than that reported by *Herrero et al.* [1993] and measured by the FPI (100-150 °K). The magnetically active runs showed slightly larger MTM features. Neither model was able to predict the premidnight MTM event. The average neutral temperatures produced by TIEGCM and MSIS differed from each other by ~200 °K

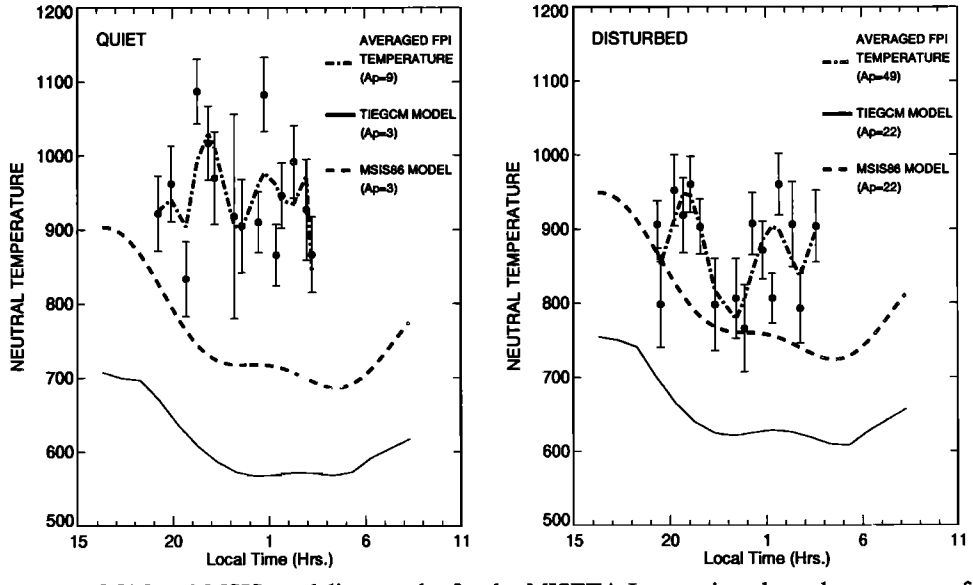

Figure 13. TIEGCM and MSIS modeling results for the MISETA-I campaign show the presence of a weak midnight MTM event (10 - 40 °K), much smaller than previously reported by *Herrero et al.* [1992] and measured by the FPI (150 - 200 °K). The mildly disturbed runs show a slightly larger MTM feature than the quiet time runs. The TIEGCM results at Ap = 3 and Ap = 22 were selected from runs closest to the actual conditions for quiet (Ap = 14) and disturbed (Ap = 49) encountered during the MISETA-I campaign. The FPI data points and error bars are shown along with a polynomial fit curve of order 7 to the data points.

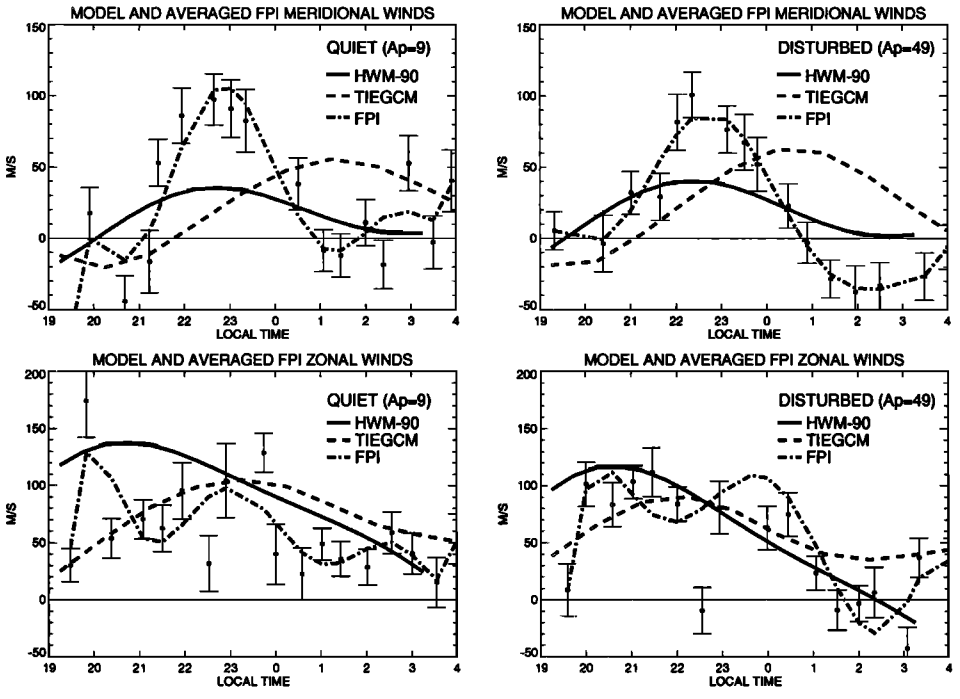

Figure 14. *Hedin* [1991] model meridional and zonal winds for both quiet (Ap=9) and disturbed (Ap=49) runs show no occurrences of reversals/abatements in the meridional winds or local minima in the zonal winds which would indicate the presence of a BW event. The quiet and disturbed cases were chosen at Ap=9 and 49, respectively, to coincide with actual conditions on September 30, October 1, 2, 8, 9, and October 3, 4, 5, 6, when the FPI observations were taken in 1994. TIEGCM results from the runs depicted in Figure 13 also fail to show wind reversals. The averaged FPI meridional and zonal wind measurements are also shown for both quiet and disturbed conditions. The meridional winds show prominent reversals from equatorward to poleward and the zonal winds show local minima in the eastward plasma drifts associated with MTM events. Polynomial fit curves of order 7 to the FPI data points are also shown.

under both active and quiet conditions. The MSIS neutral temperatures were in better agreement with the FPI measurements. Even though both models are able to produce a small MTM event for the midnight occurrence, more work needs be done in order to bring the predicted and measured magnitudes of the MTM into better agreement, as well as to account for the source of the premidnight events [*Fesen*, this issue].

The empirical wind model HWM-90 [*Hedin et al.*, 1991] was also run for both quiet (Ap=9) and disturbed (Ap=49) conditions; the results are shown in Figure 14. The HWM was unable, in both cases, to predict the reversal/abatement in the meridional winds and the local minimum in the zonal winds associated with the FPI and BW events. This is also true for the TIEGCM, with the TIEGCM winds also displaced in time by ~2 hours with respect to HWM. Only the disturbed zonal wind pattern from TIEGCM suggests a possible reversal. While plasma drifts were not measured by the Jicamarca ISR during these periods, we note that the Jicamarca radar zonal drift model does not show any evidence of local minima in the zonal plasma drifts that are driven by the thermosphere/F-region dynamo [*Fejer et al.*, 1991].

The MISETA complement of instruments can contribute substantially to future modeling studies. From the imager, nightly datasets include the time(s) of occurrence, latitude/longitude extent, and angle of orientation of individual events; day-to-day variability and seasonal occurrence patterns come from longterm observations. FPI observations provide the magnitudes of the temperature increases and the wind surges associated with MTM events. Ionosonde data provide electron density profiles of the bottomside regions ($h < h_{max}$) where the MTM airglow signatures are ultimately generated. When combined with future Jicamarca ISR observations of electric fields and temperatures, a comprehensive set of parameters will be available for modeling efforts of the pre-midnight and midnight thermal features.

Finally, the relationship (if any) between MTM events and simultaneous 6300 Å airglow depletions [*Mendillo et al.*, 1996] associated with equatorial spread- F (ESF) needs to be explored. While classic MTM signatures occur a few hours after the typical postsunset ESF onset time, post-midnight ESF events do occur, especially during geomagnetically disturbed times [*Aarons*, 1991]. Neutral wind surges are a proposed mechanism for ESF suppression [*Maruyama and Matuura*, 1984; *Mendillo et al.*, 1992], and thus there could be physical linkages between MTM and ESF patterns. For this reason, we included in the bottom panels of Figures 9 and 10 the percent occurrence of 6300 Å airglow depletions for each night as an indicator of large-scale ESF activity [*Mendillo et al*, 1996]. Moreover, during seasons when the classic MTM is preceded by an evening event, a possible MTM - ESF relationship warrants further study.

Acknowledgments. We are grateful for the assistance of D. Hallenbeck of the NASA Tracking Station in Arequipa, Peru, during

the set-up and operation of the imager and FPI. We thank F. Herrero for his valuable comments and permission for the use of his figures in this paper. This work was supported, in part, by NSF CEDAR grant ATM-9204013 and ONR grant N00014-93-1-0786, both at Boston University. The Digisonde at Jicamarca was operated under the supervision of Carlos Calderon. We thank the team at the observatory for their dedicated work. B.W.R. and J.L.S. were supported by AF contract FI9628-90-K-0029 and NSF grant ATM-9415707. C.G.F.'s work was supported by the NSF CEDAR program through grant ATM-92-03264 and NASA grant NAGW 2656; the National Center for Atmospheric Research, sponsored by the NSF, provided computing time. The FPI research was supported by grants from the CEDAR and the Aeronomy programs at the National Science Foundation, ATM-9201841 and ATM-9024951, to J.W. Meriwether and M.A. Biondi, at Clemson University and the University of Pittsburgh, respectively.

The editor thanks R. A. Behnke and another referee for their assistance in evaluating this paper.

References

Aarons, J., The role of the ring current in the generation or inhibition of equatorial F layer irregularities during magnetic storms, *Radio Sci.*, *26*, 1131, 1991.

Bamgboye, D.K., and J.P. McClure, Seasonal variations in the occurrence time of the equatorial midnight temperature bulge, *Geophys. Res. Lett.*, *9*, 457, 1982.

Baumgardner, J., B. Flynn, and M. Mendillo, Monochromatic imaging instrumentation for applications in aeronomy of the earth and planets, *Opt. Eng.*, *32*, 3028, 1993.

Behnke, R.A., and R.M. Harper, Vector measurements of *F*-region ion transport at Arecibo, *J. Geophys. Res.*, *78*, 8222, 1973.

Biondi, M.A., J.W. Meriwether, B.G. Fejer, S.A. Gonzales, and D.C. Hallenbeck, Equatorial thermospheric wind changes during the solar cycle: Measurements at Arequipa, Peru, from 1983 to 1990, *J. Geophys. Res.*, *96*, 15917, 1991.

Biondi, M.A., J.W. Meriwether, B.G. Fejer, S.A. Gonzales, and D.C. Hallenbeck, Correction to "Seasonal variations in the equatorial thermospheric wind measured at Arequipa, Peru", and "Equatorial thermospheric wind changes during the solar cycle: Measurements at Arequipa, Peru from 1983 to 1990", *J. Geophys. Res.*, *100*, 7863, 1995.

Carlson, H.C., Jr., and G. Crowley, The equinox transition study: An overview, *J. Geophys. Res.*, *94*, 16861, 1989.

Fejer, B.G., E.R. de Paula, S.A. Gonzalez, and R.F. Woodman, Average vertical and zonal *F*-region plasma drifts over Jicamarca, *J. Geophys. Res.*, *96*, 13901, 1991.

Fesen, C., Simulations of the low-latitude midnight temperature maximum, *J. Geophys. Res.*, this issue.

Friedman, J.F., and F.A. Herrero, Fabry-Perot interferometer measurements of thermospheric neutral wind gradients and reversals at Arecibo, *J. Geophys. Res.*, *86*, 5532, 1981.

Greenspan, J.A., Synoptic description of the 6300 Å nightglow near 78° west longitude, *J. Atmos. Terr. Phys.*, *28*, 739, 1966.

Harper, R.M., Nighttime meridional neutral winds near 350 km at low to mid latitudes, *J. Atmos. Terr. Phys.*, *35*, 2023, 1973.

Hedin, A.E., Extension of the MSIS thermosphere model into the middle and lower atmosphere, *J. Geophys. Res.*, *96*, 1159, 1991.

Hedin, A.E., et al., Revised global model of thermosphere winds using satellite and ground-based observations, *J. Geophys. Res.*, *96*, 7657, 1991.

Herrero, F.A., and J.W. Meriwether, Jr., 6300Å airglow meridional intensity gradients, *J. Geophys. Res.*, *85*, 4191, 1980.

Herrero, F.A., and N.W. Spencer, On the horizontal distribution of the equatorial thermospheric midnight temperature maximum and its seasonal variation, *Geophys. Res. Lett.*, *9*, 1179, 1982.

Herrero, F.A., H.G. Mayr, and N.W. Spencer, Latitudinal (seasonal) variation in the thermospheric midnight temperature maximum: A tidal analysis, *J. Geophys. Res.*, *88*, 7225, 1983.

Herrero, F.A., H.G. Mayr, N.W. Spencer, and A.E. Hedin, Interaction of zonal winds with the equatorial midnight pressure bulge in the Earth's thermosphere: Check of momentum balance, *Geophys. Res. Lett.*, *12*, 491, 1985.

Herrero, F.A., N.W. Spencer, and H.G. Mayr, Thermosphere and F-region plasma dynamics in the equatorial region, *Adv. Space Res.*, *13*, No. 1, 202, 1993

Maruyama, T., and Matuura N., Longitudinal variability of annual changes in activity of equatorial spread-F and plasma bubbles, *J. Geophys. Res.*, *89*, 10903, 1984.

Mayr, H.G., I. Harris, N.W. Spencer, A.E. Hedin, L.E. Wharton, H.S. Porter, J.C.G. Walker, and H.C. Carlson Jr., Tides and the midnight temperature anomaly in the thermosphere, *Geophys. Res. Lett.*, *6*, 447, 1979.

Mendillo, M., J. Baumgardner, X.-Q. Pi, P. J. Sultan, R. Tsunoda, Onset conditions for equatorial spread-*F*, *J. Geophys. Res.*, *97*, 13865, 1992.

Mendillo, M., M. Colerico, J. Baumgardner, D. Nottingham, Imaging science contributions to equatorial aeronomy: Initial results from the MISETA program, *J. Atmos. Terr. Phys.*, in press, 1996.

Meriwether, J.W., Jr., J.W. Moody, M.A. Biondi, and R. G. Roble, Optical interferometric measurements of nighttime equatorial thermospheric winds at Arequipa, Peru, *J. Geophys. Res.*, *91*, 5557, 1986.

Nelson, G.J., and L.L. Cogger, Dynamical behavior of the nighttime ionosphere over Arecibo, *J. Atmos. Terr. Phys.*, *33*, 1711, 1971.

Reinisch, B.W., Digisonde Network and Databasing, Rep. UAC-104, World Data Cen.A for Sol.-Terr. Phys., Boulder, Colo., 1995.

Richmond, A.D., E.C. Ridley, and R.G. Roble, A thermosphere-ionosphere general circulation model with coupled electrodynamics, *Geophys. Res. Lett.*, *19*, 601, 1992.

Spencer, N.W., G.R. Carignan, H.G. Mayr, H.B. Neiman, R.F. Theis, and L.E. Wharton, The midnight temperature maximum in the earth equatorial thermosphere, *Geophys. Res. Lett.*, *6*, 444, 1979.

Wharton, L.E., N. W. Spencer, H. G. Mayr, The Earth's thermospheric superrotation from Dynamics Explorer 2, *Geophys. Res. Lett.*, *11*, 531, 1984.

J. Baumgardner, M. Colerico, M. Mendillo, and D. Nottingham, Center for Space Physics, Boston University, Boston, MA 02215.

M. A. Biondi, Department of Physics and Astronomy, University of Pittsburgh, Pittsburgh, PA 15260

C. G. Fesen, Department of Physics and Astronomy, Dartmouth College, Hanover, NH 03755

J. Meriwether and J. Mirick, Department of Physics and Astronomy, Clemson University, Clemson, SC 29634

B. W. Reinisch and J. L. Scali, Center for Atmospheric Research, University of Massachusetts, Lowell, MA 01954

(Received November 2, 1995; revised July 23, 1996;
accepted July 24, 1996)